Research

Symmetry Breaking and Patterns

Župec Matjaž[1], Kodrin Marcel[1], Pal Kaushik[2], Kralj Samo[1,*]

1. University of Maribor, Faculty of Natural Sciences and Mathematics, Department of Physics, Maribor, Slovenia
2. University Centre for Research and Development (URCD), Department of Physics, Chandigarh University, Mohali, Gharuan, Punjab, India

* Correspondence: Samo Kralj samo.kralj@uni-mb.si

Abstract:
In the present study we analyse different patterns commonly encountered in nature. Firstly, we review patterns that display the hexagonal symmetry and triply periodic minimal surfaces. We analyse hexagonal honeycomb configurations and analyse advantages of such an architecture. Next, we use a simple Landau-type order parameter field model to illustrate how diverse patterns could be generated via the symmetry breaking mechanism.

Keywords: Hexagonal symmetry, triply periodic minimal surfaces, symmetry breaking, Landau theory, order parameter fields

Citation: Župec M, Kodrin M, Pal K, Kralj S. Symmetry Breaking and Patterns. Proceedings of Socratic Lectures. **2025**, 12(II), 127-139. https://doi.org/10.55295/PSL.12.2025.II13

Publisher's Note: UL ZF stays neutral with regard to jurisdictional claims in published maps and institu-tional affiliations.

Abstract:
We study bulk and surface phase transitions in confined nematic liquid crystals exhibiting 1st order isotropic-nematic phase transition in bulk systems. We demonstrate analytically that confinement could in general quantitatively and even qualitatively modify phase behavior. Furthermore, we show that confining substrates could enable surface phase transitions. Studied phase behaviors could be applied also to other condensed matter systems displaying 1st order continuous symmetry order-disorder phase transition if the relevant order parameter amplitude is linearly coupled to a local surface ordering field.

Keywords: Liquid crystals; Phase transition; Confined nematic liquid crystal; Surface phase transition

1. Introduction

Our surrounding world displays an enormous complexity and an infinity of diverse patterns. One would expect that it is difficult to describe key mechanisms enabling such diversity. However, it seems that the basic principles of matter originate in symmetry and symmetry breaking (Kibble, 1976; Sethna, 1992; Zurek, 1985). For example, the standard model of particles is based on symmetry breaking of local quantum fields and it seems that conserved quantities in nature could be explained by taking into account relevant systems' symmetry properties (Kibble, 1976; Sethna, 1992; Zurek, 1985).

Different materials forming solid and soft materials (Kleman et al., 2003) in our world can be viewed as being built using only three different "building blocks", i.e., electrons, protons and neutrons. These are combined in atoms following quantum mechanical rules and furthermore, atoms could assemble in further higher-hierarchical configurations. Furthermore, it seems that key natural behaviors could be explained using geometrical concepts (Imry and Ma, 1975; Kibble et al., 1976; Sethna, 1992; Zurek, 1985).

In the following we present some i) systems exhibiting hexagonal symmetry or ii) systems, that are making use of the minimal surface principle to illustrate how structures are related to different emerging functionalities.

1.1. Hexagonal lattices

We first focus on hexagonal lattices which are ubiquitously realised in nature. The typical lattice consists of hexagons as shown in **Figure 1**. One see that blue and yellow coloured elements, which form the lattice, are not connected the same way. Blue atoms have a neighbour horizontally to the right and two more diagonally to the left. The situation is inversed for the yellow ones. This lattice can be described in terms of three base vectors $\mathbf{a}_i$, via which each lattice point could be located. Hexagons are also one of three shapes that can cover a 2D plane just by themselves, the other two being triangles and squares. But hexagonal tiling is the closest packing way to arrange circles in two dimensions (the best way to divide a surface into regions of equal area with the least total perimeter) which was proven by Thomas C. Hales (Hales, 2001).

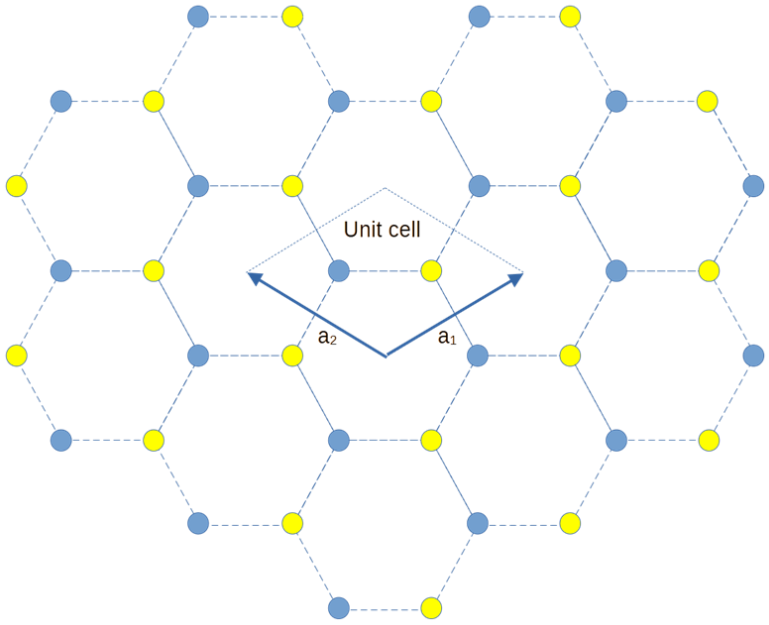

Figure 1: Hexagonal lattice in 2D in which we show the unit cell and the corresponding base vectors.

Hexagonal lattices are widely used in various applications. One example are hexagonally shaped fence from galvanized steel, also known as the chicken mesh. Furthermore, Mebrahtom et al. (2024) compared the chicken mesh with welded square mesh and expanded metal mesh in tests, where they added mentioned meshes to concrete beams. They tested their energy absorption (free fall), compressive strength (capacity of a material to withstand loads that try to reduce its size) and flexural strength (the ability of a material to withstand bending under the application of external force). The chicken mesh outperformed the other two in all the tests. A single layer increased the flexural strength of a beam by 8 times (compared to 6 and two times for other two), reduced the compressive strength by less than 1% (better than over 1% for welded mesh and 8% reduction for expanded mesh), while it could absorb 255 J of energy from free fall (compared to 198 J and 188 J for other two). That in combination with its cheap price makes it a great contender for reinforcing concrete beams.

Furthermore Carbon, which is the base of life on Earth, is often found forming hexagonal lattices in forms like graphite, graphene or nanotubes. Latter two forms have high ultimate tensile strength, up to 130,000 MPa for graphene (Lee et al., 2008) and (theoretically) up to 300,000 MPa for nanotubes (Yu et al., 2000). For comparison, different forms of steel can be found to have around 2,000 MPa. Graphite on the other hand is thought to be one of the first crystals to ever condense, possibly only behind diamond (Hazen et al., 2013). Graphite could be transformed into diamond only under pressure of a few GPa, depending on the temperature (1 GPa = 10,000 bar). At 5000 K and 12 GPa a triple point of carbon was found (where carbon is present in liquid, diamond and graphite form)(Bundy et al., 1994). One layer of graphite yields graphene, the miracle material. This is partly due to the fact that for decades, it was believed that 2D materials were non-existent in nature (Ding et al. 2019). Part of the problem is that the bending stiffness (the resistance of a member against bending deflection/deformation) based on continuum mechanics theory is proportional to the cubic power of the thickness. Therefore it should be negligible for 2D materials. But the discovery of graphene in 2004 changed the narrative. Ding et al. (2019) found that when it comes to 2D lattices, hexagonal is superior to triangular and square. This is because, in contrast to the other two, the hexagonal lattice experiences variation of the bond angles during bending, providing finite bending stiffness and thus great stability. With their model they also found that repulsive moment of atoms arranged in a hexagonal lattice increases the structural stability of the lattice. The same cannot be said for triangular and square lattices, as their attractive inner moment renders them unstable, which was shown by using the same model.

Back to graphene, it is said to conduct electricity better than any other material known to science, and is known for its material strength. Its heat conductivity was also believed to be beyond any other material, however Han and Ruan found that this is not the case (Han and Ruan, 2023). Many papers put the thermal conductivity of graphene between 3,000 and 5,000 W/mK, but Ruan's team measured it to be around 1,300 W/mK, which falls short of diamond (2,000 W/mK). This figures are all huge, as thermal conductivity of iron for example is around 80 W/mK at room temperature. But graphene is still the front runner for superconductivity of electricity. Superconductivity is the phenomenon when the electrical resistance of the material drops to zero and magnetic fields are expelled from it. This only happens once the temperature of the material drops under the critical temperature. One way to make graphene into a superconductor is to take two sheets of the magical material and twist them for the "magic angle". At the temperature of under 1,7 K under an angle of roughly 1.05° the material becomes superconducting. The term magic angle was suggested in 2011 (Bistritzer and MacDonald, 2011), although it wasn't known back then it would lead to superconductivity, rather it was known that band structures appear in which electrons are in a way isolated from each other. More options for superconductivity are made with more layers of graphene. With three layers, twisted by 1.5° relative to each other, the material becomes superconductive at roughly 2.5 K. The mechanism behind this exact observation remains unknown (Garisto, 2023).

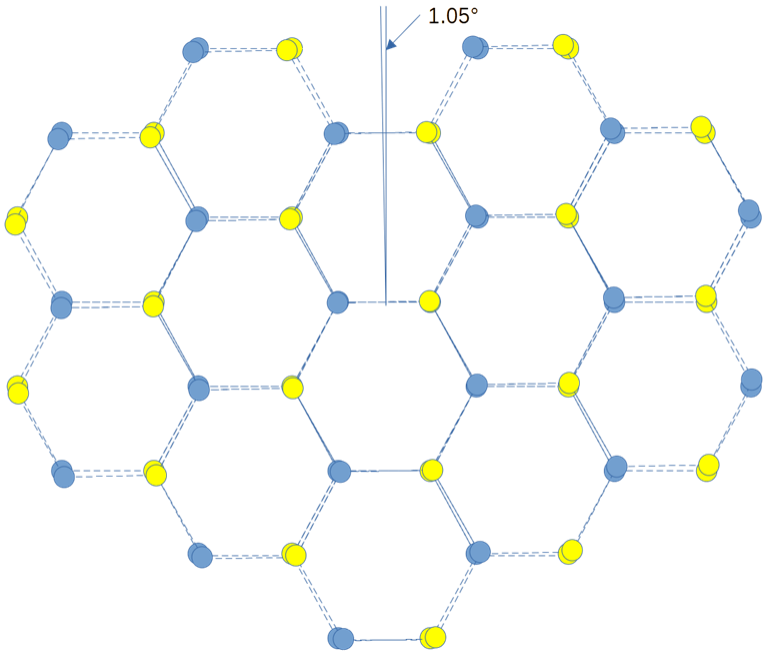

Figure 2: Two graphene lattices, twisted by 1.05°.

Finally, that same lattice that makes concrete stronger and graphene into a miracle material, is also used by animals such as bees. They build cylindrical cells that later transform into hexagonal prisms, achieving a maximal surface/perimeter ratio, through a process that it is still debated, even though the honeycomb has been a subject of thought since the antiquity, when it caught the eye of the Roman philosopher Marcus Terentius Varro. It could be explained partially by action of physical forces, as well as behaviour of bees, as they use their legs to measure distances (Nazzi, 2016). They also use their bodies to keep the temperature of the wax at around 35 °C, which is a bit below the temperature where wax exists in a liquid-solid equilibrium at 40 °C, which still allows bees to modify wax in hexagonal patterns, suggesting that behaviour of bees could be the answer (Bauer and Bienefeld, 2012). Further articles (Nazzi, 2016) talk about a similar idea of bees themselves creating hexagonal pattern. The bees were shown to mostly start constructing a new cell from the groove formed by the two previous cells. However, bees also build honeycombs starting from many different points, and this is where constructing a perfect hexagonal lattice becomes impossible (Smith et al., 2021). But they have evolved to change their behaviour in order to sew parts of the honeycomb together with pentagons and heptagons. They can also tilt individual hexagons in order to fill out the pattern. Keep in mind that the bees have limited global awareness and make decisions based on local information. And they still get it right, so we can conclude that bees are some of the most skilled architects out there.

1.2. Triply periodic minimal surfaces

Triply periodic minimal surfaces or TPMS are structures with two main defining features. The first is their minimal surface trait. In topology, for a surface to be deemed minimal, it has to satisfy a simple requirement: the mean curvature at each point on the surface is zero. In other words, they are equally convex and concave at all points or saddle-like or hyperbolic in shape. The name comes from the fact that, given a fixed boundary, their surface is the smallest compared to other surfaces constructed under the same boundary conditions. The second feature is the triply periodicity. This means that the structure has three base vectors and thus repeats periodically in 3 directions or is in other words a three-dimensional structure. Most TPMS are non-intersecting and divide space into separate volumes. These volumes can be tailored to be different in size in relation to each other. In our cases there will only be two of these volumes.

There are many different types of TPMS with new ones still being investigated or just theorized. The main types of TPMS structures are the primitive (P), diamond (D) and gyroid (G) types. They can be depicted in multiple ways. The simplest is in the form of a skeletal structure. The skeletal structures represent the volumes that are separated by the surfaces. These lattices are the same in our cases, with them being rotated and intertwined. The primitive TPMS has a simple cubic skeletal structure that represents one of the volumes in red and another simple cubic structure that represents the other volume in blue as seen in **Figure 3**.

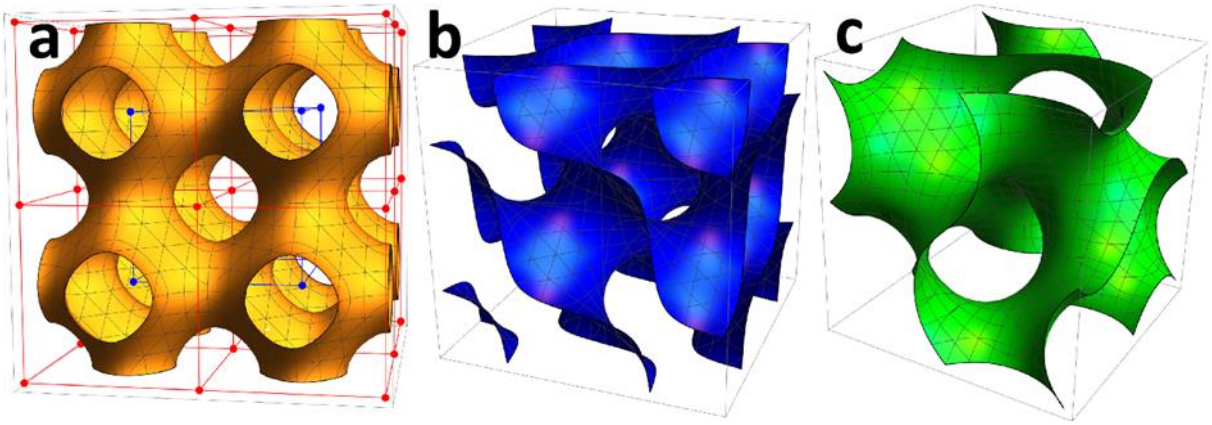

Figure 3: Examples of TPMS: a) primitive TPMS with lattices as depiction of volumes; b) diamond TPMS; c) gyroid TPMS.

In the following we list some of peculiar features enables by TPMS structures. There are two ways of creating a coloured surface. The first is with the use of dyes. These work by simply absorbing or reflecting certain parts of the spectrum of visible light, due to their chemical make-up. The second are structural colours. These are produced due to the way material is shaped. These structures use physical phenomena such as interference or diffraction to selectively reflect different wavelengths of light at different intensities. In the case of TPMS the phenomenon that we see happen is mainly Bragg scattering. Bragg scattering is a phenomenon that was first observed in atomic lattices. The interaction between the atoms and the waves, when they enter a crystal, can be modelled by creating parallel planes at a distance d from one another off which light would bounce. If the wavelength of light and angle of the incident waves is just right the constructive interference occurs. Otherwise, we get destructive interference or there is no change in intensity. This means that a peak of intensity of certain wavelengths of light is created. The peak is what we primarily then interpret as the colour of the object. The colour of parts of the wing or even the whole wing can change as we view it from different directions, because of the angle dependence of the incoming and thus reflected light. We also see a metal-like shine due to the method of colouring, that is not common in dyes.

The coloured part of butterfly wings are really scales, that are attached to the main body of the wing. Butterflies use many different techniques to attain the colours of these wings. In some cases, they use simple dyes and in others they use different types of structural colouring methods. What we do see is that in the latter cases, traditional dyes like melanin are also in some cases used as a base. These dyes cause the structural mechanisms to work better, as they also help to absorb light.

Firstly, to determine what method of colouring is used. Saranthan et al. used a method of imaging called small angle X-ray scattering or SAXS to take measurements of the nanostructure of certain species of butterfly wings, which were previously thought to have TPMS structures, to determine which type of structure they use. They found that the five species they imaged all used the gyroid structure. The structure is comprised of chitin and air. They also then, using this information, predicted what the reflective spectra of the butterfly wing scales would be. They found that the real and simulated spectra both match up well (Saranathan, 2010).

Beetles also use TPMS structures, that are created in the form of dots on their carapace, to display colours. Galusha (2008) investigated the scales of the weevil Lamprocyphus augustus using high-resolution imaging techniques and simulations to determine that these weevils use a diamond TPMS structure as their colouring method. They also found that these structures have a sort of grainy composition to them. The structure is not perfect like we would expect to see in a crystal but shows domains of periodicity. They also found that it is thanks to these non-uniform assemblies that the beetles have a near angle-independent coloration, which means that you can see these colours from any angle (Galusha, 2008).
TPMS is encountered also in the mitochondria of amoeba (Chaos carolinensis). The cell is commonly known as a sort of ball of living material floating around in an environment. The only thing dividing these two environments is the membrane on the outside of the cell. And just as we have smaller masses called organs inside of us that have their own specific function and are separated from the rest of the body by different layers, so does the cell too have its own organelle. These have their own outer and inner layers. These layers have recently in some cases been found to be cubic membrane structures which are analogous to TPMS. Examples from the work of Landh included the smooth endoplasmic reticulum, mitochondrial inner membrane and chloroplast thylakoid membranes (Landh, 1995). Deng et al. have used transmission electron microscopy and simulations of TPMS structures to find the structure used in the cells of the giant amoeba Chaos carolinensis (Deng et al., 2017). They found that the structure best aligns with a double diamond structure, which is a more complex variant of the normal diamond structure. The exact reasons for these structures are still not fully known although a few theories and advantages have been found. One theory, as proposed by Deng et al. is that because these amoebae do not have a way of going into a dormancy state, the mitochondria constantly must produce energy (Deng et al., 2017). The most common source of this energy during starvation are the membranes of the mitochondria. Because the mitochondria still need to uphold a certain surface to volume ratio while their membrane is being consumed, they take the form of a very efficient structure (Deng et al., 2017).
Deng et al. have also found another possible use of these structures in mitochondria. They tested the oxidative damage that was dealt to RNA in the presence of two different mitochondria structures. They used the mitochondria of a 7-day starved amoeba and those from a mouse liver, which do not have TPMS structures. As another control, they tried comparing the effects from the mitochondria of starved and non-starved amoeba. The RNA with the cubic structure mitochondria had accumulated less damage than the RNA in the other two cases. Thus we can assume there to be another reason for mitochondria to take the cubic membrane structure (Deng et al., 2017).
In this contribution we present two different illustrations of geometrically driven phenomena. Firstly, we consider hexagonal patterns engineered by bees and analyze resulting beneficiaries. Next, we present a simple minimal model which explains how symmetry breaking could generate attractive or repulsive interactions among "objects". We demonstrate that infinity of different configurations could emerge although equilibrium configurations of such unperturbed systems are expected to be featureless.

3. Methods

We use a simple Landau-type approach in which phase and structural behaviors are described in terms of order parameter field (Kleman et al., 2003; Sethna, 1992). We consider a 3D system exhibiting a continuous symmetry breaking phase transition on varying a relevant driving parameter (temperature in our case). We assume that a long-range axial orientational order is formed in the symmetry broken phase, which is spatially homogeneous in bulk (i.e., large enough unperturbed system where boundary conditions could be neglected) equilibrium. Hence, we focus on a system which exhibits isotropic symmetry (i.e., it does not possess any kind of order) in the higher temperature phase and below the critical temperature T_c displays a long-range orientational order. The latter is in bulk equilibrium spatially homogeneous along an arbitrary symmetry breaking direction.
For example, such a phase transition could be realized in thermotropic nematic liquid crystals (Kleman et al., 2003) (NLCs) which we use as an illustrating "toy model". Namely, the theory of NLCs is relatively well developed (Kleman et al., 2003) and phenomena

analyzed in this contribution could be experimentally observed. For simplicity we consider LCs formed by anisotropic rod-like molecules, whose local order could be presented by an axial field, whose orientation is commonly referred to as the nematic director field $\hat{n}$. The states $\pm\hat{n}$ are physically equivalent to mimic the axial symmetry. In thermotropic NLCs the orientational describing local uniaxial order is given by the symmetric and traceless tensor order parameter which can be expressed in terms of $\hat{n}$ as

$$\underline{Q} = S\left(\hat{n}\otimes\hat{n} - \frac{\underline{I}}{3}\right) \tag{1}$$

The additional quantity in Eq.(1) is the scalar nematic order parameter S which describes the degree of orientational order. In the isotropic phase, which exhibits isotropic symmetry and is stable above the critical temperature T_c, the nematic order is absent and S=0. In the uniaxial nematic phase, which is stable below T_c, S>0 and in bulk equilibrium the tensor order parameter is spatially homogeneous.
For general conditions the order parameter field spatial configuration minimizes the free energy F which we express as

$$F = \iiint (f_c + f_e)dv + \sum_j \iint f_i^{(j)} da. \tag{2}$$

The first integral in Eq.(2) is carried out over the LC body, where dv stands for the volume element, f_c is the condensation and f_e elastic free energy density. The second integral sums contributions at interfaces of a confining surface (or surfaces) and other interfaces, for example, LC-immersed particle interfaces. The quantity $f_i^{(j)}$ describes the local interaction free energy contribution at j-th interface and da is the interface surface element. In our analysis we will assume that either super-micrometre (colloids) or nano-sized objects (nanoparticles) are immersed in LC liquid. Such additional symmetry breaking sources could enormously increase the pallet of different stable NLC configurations. We use the simplest minimal model which is needed for our analysis in which we express the free energy densities entering Eq.(2) as

$$f_c = \frac{3}{2}a_0(T - T^*)\mathrm{Tr}\underline{Q}^2 - \frac{9}{2}b\ \mathrm{Tr}\underline{Q}^3 + \frac{9}{4}c\left(\mathrm{Tr}\underline{Q}^2\right)^2 = a_0(T - T^*)S^2 - b\ S^3 + cS^4, \tag{3a}$$

$$f_e = \frac{L}{2}\left|\nabla\underline{Q}\right|^2 \sim \frac{L}{2}|\nabla S|^2 + \frac{K}{2}|\nabla\hat{\mathrm{n}}|^2, \tag{3b}$$

$$f_i^{(j)} = -\frac{3}{2}w\hat{\mathrm{e}}.\underline{Q}\hat{\mathrm{e}}, \tag{3c}$$

The condensation term determines the equilibrium degree of nematic order $S = S_{eq}$ in bulk equilibrium, where a_0, T^*, b and c are positive material dependent constants (Kleman et al., 2003). The minimization of Eq. (3a) yields

$$S_{eq}/S_0 = \frac{3+\sqrt{9-8\frac{T-T_c}{T_c-T^*}}}{4} \tag{4}$$

for $T \le T_c$ where $S_0 = \frac{b}{2c} = S_{eq}(T_c)$ and $T_c = T^* + \frac{b^2}{4a_0c}$.

The elastic term penalizes spatially non-homogeneities in $\nabla\underline{Q}$, where L>0 and $K \sim LS^2$ stand for the representative elastic constant resisting spatial variations in S and $\hat{n}$, respectively.
The interfacial term enforces the alignment along the so-called local easy direction $\hat{e}$ if the anchoring constant w is positive.

4. Results

Below we present our analysis. We first show key factors why bees engineer hexagonal patterns. Next we show using our simple modelling how diverse patters could be obtained in nature via symmetry breaking mechanisms.

4.1. Hexagonal honeycombs

Figure 4: An example of honeycomb. There are no shapes other than hexagons, as there is a matrice below for bees to use.

We analysed a honeycomb shown in **Fig.4** of area 37.6 cm times 12.9 cm. We measured that the base of one hexagonal cell is 3.25±0.06 mm. We found out that the combined length of all the hexagons in the honeycomb is around 17.2 m, which is way more than one would anticipate. The area of the cell is $A = \frac{3\sqrt{3}a^2}{2}$, where a is the base. This gives A=27±1 mm^2. From that we can conclude that the side length of a square with the same area is around 5.2 mm. If bees used squares instead of hexagons, then the total length of the perimeter would be 18.2 m. So we can see that the Honeycomb conjecture holds true. If we assume the height of the cells to be 2.8 cm and the width of the walls to be 0.3 mm, than we can calculate that the bees save around 8 cm^3 of wax per honeycomb.

4.2. Symmetry breaking generated patterns

In the following we illustrate how the simple Landau-type approach presented reveals that simple mechanisms could generate several patterns and interactions that we observe in nature.

As already mentioned, the free energy given by Eq.(2) favors spatially homogeneous patterns aligned along a single symmetry breaking direction in the absence of interfacial interactions that would break the symmetry. We emphasize that there exists an infinite number of equivalent equilibrium states each pointing along a different symmetry direction. The competition between these states is crucial for the diversity of different complex patterns that could emerge.

We first consider simple possible excitations in a bulk equilibrium nematic structure where we set $f_i^{(j)} = 0$. For simplicity we restrict to 2D and parametrize the director field by an angle θ as

$$\hat{\mathrm{n}} = (\mathrm{Cos}(\theta), \mathrm{Sin}(\theta)) \tag{5}$$

and assume a constant value of S equal to S_{eq}, given by Eq.(4) which minimizes f_c. Minimization of the free energy yields the Euler-Lagrange equation

$$\nabla^2\theta = 0 \tag{6}$$

and the possible solutions read [17]

$$\theta = m\ \ \mathrm{ArcTan}\left(\frac{y}{x}\right) + \theta_0 = m\ \ \mathrm{ArcTan}(\varphi) + \theta_0. \tag{7}$$

Here $\varphi = \mathrm{ArcTan}\left(\frac{y}{x}\right)$ is the azimuthal angle in polar coordinates, m is the so-called winding number and θ_0 is a constant. Note that the condition $\hat{\mathrm{n}}(\varphi = 0) = \hat{\mathrm{n}}(\varphi = 2\pi)$ must be obeyed, which restricts values of m to half integers (due to the axial symmetry the states $\pm\hat{n}$ are equivalent):

$$m \in \{0, \pm\tfrac{1}{2}, \pm 1, \pm\tfrac{3}{2}, \dots\} \tag{8}$$

Solutions corresponding to $m = 0$ represent the competing equilibrium states $\hat{\mathrm{n}}_{eq} = (\mathrm{Cos}(\theta_0), \mathrm{Sin}(\theta_0))$ aligned along a symmetry breaking direction given by $\theta = \theta_0$. Furthermore, the solutions with $m \neq 0$ correspond to topological defects (TDs) whose centers are localized at $(x,y)=(0,0)$. Some examples are shown in **Figure 5**. In 2D the winding number m is equivalent to the so-called topological charge, which is a conserved quantity, similarly as the electric charge in electrostatics. Namely, if the boundary conditions along any closed path are fixed then the total value of m within the enclosed region is conserved. Furthermore, defects bearing $m>0$ and $-m$ are referred to as defects and antidefects. Such a pair experiences mutual attraction and tends to annihilate into a defectless state. **Figure 6** illustrates cases including more TDs. Because Eq.(6) is linear, linear combinations of solutions are also solutions. A pattern emerging from N defects, where an i-th defect possessing a charge x_i is centered at (x_i, y_i), could be described by

$$\theta = \sum_{i=1}^{N} m_i \ \mathrm{ArcTan}\left(\frac{y-y_i}{x-x_i}\right) + \theta_0. \qquad (9)$$

For example, the top two patterns in **Figure 5** present defects bearing m=1/2 (left) and m=-1/2 (right). These two defects act as a pair {defect, antidefect} and tend to mutually annihilate into a defectless state in which the director pattern is spatially homogeneous. The first left panel of **Figure 6** illustrates such a nearby pair. Note that the total charge of the system equals to zero and such a state is topologically equivalent to a spatially homogeneous pattern (i.e., ground state) which has the lowest free energy. Therefore, if one starts with a pattern of N defects, where the total topological charge of the system equals to zero, then such a pattern would gradually transform into a defectless ground state via annihilation of defects and antidefects. This behavior is reminiscent to the system of particles and antiparticles bearing positive (e>0) and negative (e<0) electric charges, where m mimics the role of e. Similar as in electrostatics, TDs bearing opposite (same) sign mutually attract (repeal) and the total charge is in both cases conserved.

How a complex nonuniform pattern could be stabilized? Let us assume that colloids or nanoparticles are present in the system, to which we henceforth refer as particles. For simplicity we assume that particles are spherical and their interaction with the enclosing LC is described by Eq.(3c). If the coupling constant is relatively weak, such particles do not strongly affect the surrounding LC as it is schematically depicted in **Figure 7a**. Let us assume that easy axes of particles are radially oriented, so that particles would act similarly as m=1 defects (see the TD pattern in the left middle panel of **Figure 5**) on larger length scales in the strong interaction limit w>>0. In such case the particle will create an antidefect bearing m=-1 in order to reduce the total deformation in the system. This is illustrated in **Figure 7b**, where the far nematic director field (with respect to the particle position) tends to be spatially homogenous along the vertical direction. Note that in three dimensions the accompanying antidefect (described by m=-1 in 2D) could form a topologically equivalent defect line which is shown in **Figure 7c**. However, despite topologically equivalent structures shown in **Figure 7b** and **Figure 7c**, the symmetry and resulting interactions strongly differ. Namely, in these figures the effective nematic pattern acts as a topological dipole (**Figure 7b**) and topological quadrupole (**Figure 7c**). Therefore, in the presence of several particles different deformed nematic patterns could emerge depending on particles' geometries (size, shape) and particle-LC interaction character.

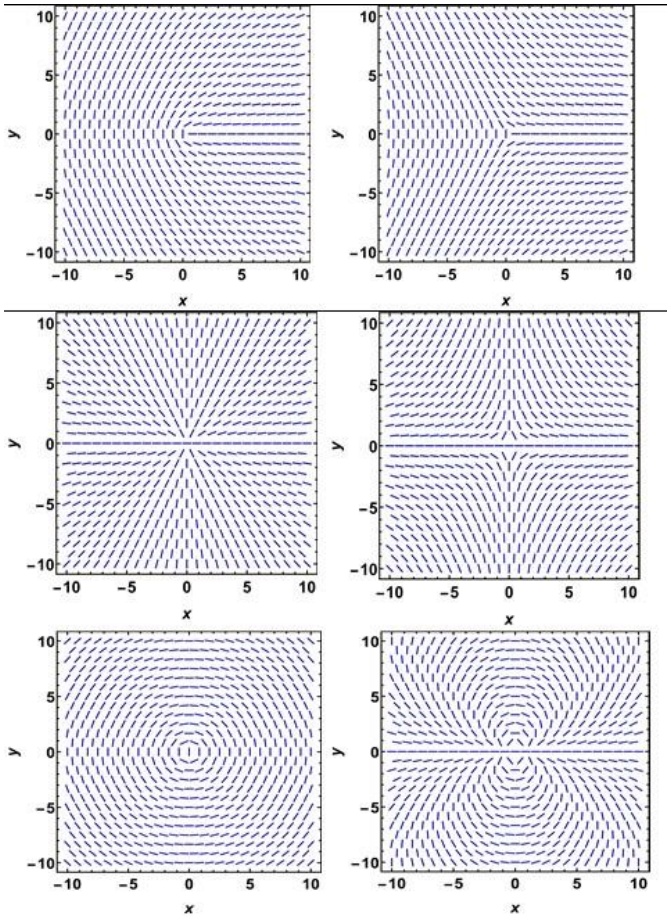

Figure 5: Different topological defects centred at (*x*=0,*y*=0). In most case $\theta_0 = 0$ if not stated otherwise. Top panel: (left) *m*=1/2; (right) *m*=-1/2. Middle panel: (left) *m*=1; (right) *m*=-1. Bottom panel: (left) *m*=1, $\theta_0 = \pi/2$; (right) *m*=2.

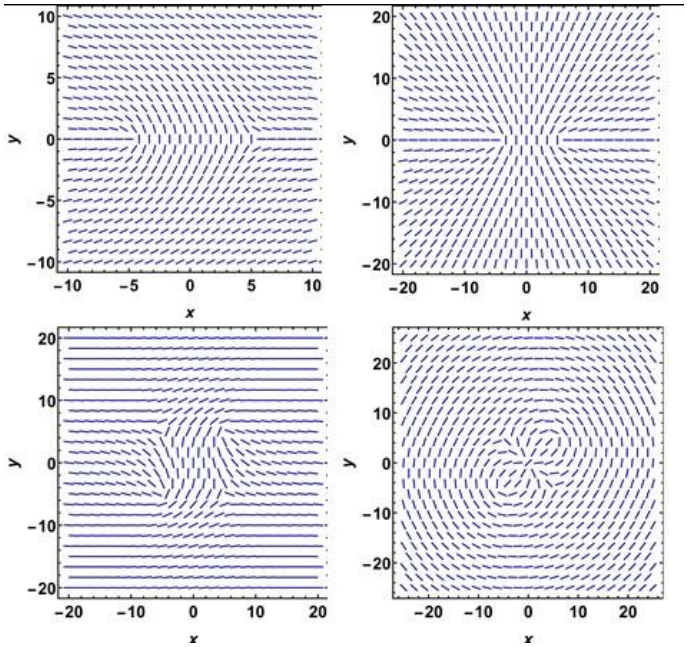

Figure 6: Assemblies of TDs. Their total charge is given by m_{tot}. Top panel: (left) a pair {*m*=1/2,*m*=-1/2}, $m_{tot} = 0$; (right) two *m*=1/2 TDs, $m_{tot} = 1$. Bottom panel: (left) two anti-parallel pairs {*m*=-1/2,*m*=1/2} of TDs, $m_{tot} = 0$; (right) four $|m|$=1/2 and one *m*=1 TDs, $m_{tot} = 1$.

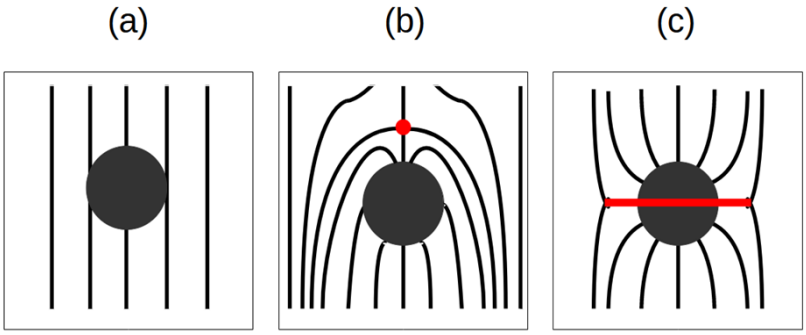

Figure 7: A spherical particle immersed in a LC body. (a); w=0, spatially homogeneous nematic structure. In (b) and (c) we have strong interfacial coupling and consequently an antidefect needs to be introduced in LC patterns. Their cores, where nematic order is essentially melted, are red coloured; (b): point-like antidefect and dipolar LC symmetry; (c): line-like antidefect and quadrupolar LC symmetry.

Let us estimate the condition in 3D for which a configuration in **Figure 7c** is more favorable than an undistorted pattern like the one shown in **Figure 7a**. For this purpose, we roughly compare LC free energy penalties of the competing configurations. In the undistorted pattern there are no elastic penalties. However, the surface penalty is relatively high, because LC molecules are not aligned along directions favored by $f_i^{(j)}$. The total free energy penalty of the system is then roughly given by

$$F^{(non)} \sim w \; A \qquad , \tag{10}$$

where $A = 4\pi R^2$ is the surface of the particle of radius R and the superscript (non) refers to the undistorted LC pattern. On the other hand, in **Figure 7c** the interfacial conditions are perfectly obeyed and consequently a line antidefect of radius r must be formed in order to immerse the distorted LC region in an uniform nematic alignment. We assume that the key "volume" LC penalty comes from the melting of LC order at the defect line. Namely, at the center of defects the orientational order is not uniquely defined and must be locally melted. The radius of the melted region is roughly given by the so-called nematic order correlation length $\xi \sim \sqrt{L/(a_0(T_{IN} - T))}$ (Kleman et al., 2003). Therefore, the dominant free energy contribution of the distorted configuration reads

$$F^{(dis)} \sim a_0(T_{IN} - T) S_0^2 (2\pi r)(\pi \xi^2) \sim L S_0^2 4\pi r. \tag{11}$$

In this estimate we took into account Eq.(4) and expressed the resulting free energy close to the phase transition temperature and (dis) labels the distorted pattern. Assuming $r \sim R$ we obtain from the "compromise" criteria $F^{(dis)} \sim F^{(non)}$ the condition

$$\mu = \frac{Rw}{K} \sim 1 \qquad . \tag{12}$$

where $K = LS_0^2$. Therefore, in the regime $\mu < 1$ and $\mu > 1$ the undistorted and distorted patterns are realized, respectively.

5. Discussion

Our study illustrates that symmetry breaking mechanisms could very efficiently generate various complex patterns particularly in system where a continuous symmetry is broken. In such cases systems are very susceptible to various perturbations, because they have in general a rich palette of different ways to respond. Furthermore, continuous symmetry breaking enables formation of topological defects (Kibble, 1976; Sethna, 1992; Zurek, 1985). Such excitations in many cases behave like flexible bodies and one can assign to them topological charges which are conserved quantities. In interactions and recombination of such entities could be predicted based on group theory (Kibble, 1976; Sethna, 1992; Zurek, 1985) and systems exhibiting similar symmetries share several similarities in mathematical behavior although they could be physically completely different. Axial symmetry enables in

addition to point defects also topologically stable line defects (Bradač et al., 2011; Kleman et al., 2003). For example, in magnetic systems, where a vector order parameter could serve as the order parameter, line defects could not be topologically stable. Therefore, systems like nematic liquid crystals could for this purpose exhibit even larger complexity than for example magnetic systems, in which several pioneering solid state studies have been made (Imry and Ma, 1975; Sethna, 1992).

We demonstrated that different patterns in nematic liquid crystals can be efficiently formed by dispersing various particles within them. We illustrated that both geometry, in particular topology, and interfacial interactions play an important role. However, the history of samples could be another rich generator of additional patterns which we did not address. For example, if the isotropic-nematic phase transition is fast enough then a dense tangle of topological defects is formed just after the transition. Namely, if the phase transformation is too fast for different regions to communicate, in distant parts the symmetry is in general broken in different directions. In such cases the concentration of TDs strongly depend on the quench rate (Kibble, 1976; Zurek, 1985; Bradač et al., 2011) (i.e., the time in which the transition is realized). If particles are present in LC medium, then additional different and complex configurations could emerge whose average behavior could be tuned by diverse tunning parameters (Bradač et al., 2011; Pišljar et al., 2024; Ranjkesh et al., 2014) (e.g, quench rate, topology of particles, geometrical properties of particles, LC confining geometry…). This will be the focus of our future planned research.

6. Conclusions

We analysed different patterns that are commonly realised in nature. We reviewed configurations displaying hexagonal symmetry and exploiting triply periodic minimal surfaces in different physical systems. Furthermore, key advantages of such patterns are reported. We studied in more detail honeycomb hexagonal structure and show the key advantages of such configurations. In addition, we presented a simple Landau-type model to show how a relatively simple symmetry breaking mechanism could generate a rich diversity of different patterns. In our illustration we used nematic liquid crystal pastern as an experimentally approachable system where such phenomena could be directly observed using relatively simple optic methods (e.g., polarising microscopy).

Funding: This research was supported by Slovenian Research Agency through the pro-ject J2-4447.

Conflicts of Interest: The authors declare no conflict of interest.

References

1. Bauer D, Bienefeld K. Hexagonal comb cells of honeybees are not produced via a liquid equilibrium process. Naturwissenschaften. 2012;100:45–49. doi:10.1007/s00114-012-0992-3
2. Bistritzer R, MacDonald AH, Moiré bands in twisted double-layer graphene. Proc Natl Acad Sci U.S.A. 2011; 108:12233-12237. https://doi.org/10.1073/pnas.1108174108
3. Bradač Z, Kralj S, Žumer S. Early stage domain coarsening of the isotropic-nematic phase transition. The Journal of Chemical Physics. 2011;135(2):024506. https://doi.org/10.1063/1.3609102
4. Changgu Lee et al. Measurement of the Elastic Properties and Intrinsic Strength of Monolayer Graphene. Science. 2008;321:385-388. DOI:10.1126/science.1157996
5. Deng YA, Three-dimensional periodic cubic membrane structure in the mitochondria of amoebae *Chaos carolinensis*. Protoplasma. 1998;203:16--25. doi:10.1007/BF01280583
6. Deng YA,Evaluation of radical scavenging system in amoeba *Chaos carolinense* during nutrient deprivation. Interface Focus. 2017;7(4):20160113. doi:10.1098/rsfs.2016.0113
7. Ding H, Zhen Z, Imtiaz H, et al. Why are most 2D lattices hexagonal and the existence possibility of various 2D materials predicted by a simple mechanics model. Extreme Mechanics Letters, 2019:100507. doi:10.1016/j.eml.2019.100507
8. Bundy FP, Bassett WA, Weathers MS, et al. The pressure-temperature phase and transformation diagram for carbon; updated through 1994. Carbon. 1996;34:141-153. https://doi.org/10.1016/0008-6223(96)00170-4

9. Galusha JW. Discovery of a diamond-based photonic crystal structure in beetle scales. Phys Rev E. 2008;77(5): 050904. doi:10.1103/PhysRevE.77.050904
10. Garisto D. New demonstrations of superconductivity in multilayer stacks of graphene continue to emerge, even as researchers struggle to explain how it all works. Physics Today. 2023: https://doi.org/10.1063/PT.6.1.20230414a
11. Hales T. The Honeycomb Conjecture. Discrete Comput Geom. 2001:1–22. https://doi.org/10.1007/s004540010071
12. Han Z, Ruan X. Thermal conductivity of monolayer graphene: Convergent and lower than diamond. Phys Rev B. 2023;108:12. https://link.aps.org/doi/10.1103/PhysRevB.108.L121412
13. Hazen RM, Downs RT, Kah L, Sverjensky D. Carbon Mineral Evolution. Reviews in Mineralogy and Geochemistry. 2013;75(1):79–107. doi:10.2138/rmg.2013.75.4
14. Imry Y, Ma S. Random-Field Instability of the Ordered State of Continuous Symmetry. Physical Review Letters, 1975; 35(21):1399–1401. https://doi.org/10.1103/PhysRevLett.35.1399
15. Kibble TWB. Topology of cosmic domains and strings. Journal of Physics A: Mathematical and General, 1976;9(8):1387–1398. https://doi.org/10.1088/0305-4470/9/8/029
16. Kléman M, Lavrentovich OD, Friedel J. Soft matter physics: An introduction. Springer, 2003.
17. Landh T. From entangled membranes to eclectic morphologies: cubic membranes as subcellular space organizers. FEBS Letters, 1995, 369(1), 13-17. doi:10.1016/0014-5793(95)00660-2
18. Landh T. Cubic cell membrane architectures. Taking another look at membrane bound cell spaces. Thesis. Lund University, Sweden. 1996, pp:188. Available at https://www.lunduniversity.lu.se/lup/publication/41686fe3-8ab2-445d-8e70-c43747087210. Accessed on 9.3.2025.
19. Mebrahtom M, Fissha Y, Ali M, et al. Comparative study of eco-friendly wire mesh configurations to enhance sustainability in reinforced concrete structures. Sci Rep. 2024;14:8818. https://doi.org/10.1038/s41598-024-59050-2
20. Yu MF, Lourie O, Dyer MJ, et al. Strength and Breaking mechanism of multiwalled carbon nanotubes under tensile load.science. 2000; 287,637-640. DOI:10.1126/science.287.5453.637
21. Nazzi F. The hexagonal shape of the honeycomb cells depends on the construction behavior of bees. Sci Rep. 2016;6,28341. DOI: 10.1038/srep28341
22. Pišljar J, Nych A, Ognysta U, et al. Dynamics and Topology of Symmetry Breaking with Skyrmions. Physical Review Letters, 2024;132(17):178101. https://doi.org/10.1103/PhysRevLett.132.178101
23. Ranjkesh A, Ambrožič M, Kralj S, Sluckin TJ. Computational studies of history dependence in nematic liquid crystals in random environments. Physical Review E. 2014;89(2):022504. https://doi.org/10.1103/PhysRevE.89.022504
24. Saranathan V, Osuji CO, Mochrie SGJ, Prum RO. Structure, function, and self-assembly of single network gyroid (I4132) photonic crystals in butterfly wing scales. Proceedings of the National Academy of Sciences of the United States of America (PNAS). 2010;107(26),11676--11681. doi:10.1073/pnas.0909616107
25. Sethna JP. Order Parameters, Broken Symmetry, and Topology. arXiv:cond-mat/9204009v3. 2009: https://doi.org/10.48550/ARXIV.COND-MAT/9204009
26. Smith ML, Napp N, Petersen KH, Imperfect comb construction reveals the architectural abilities of honeybees, Proc Natl Acad Sci USA. 2021;118(31): e2103605118. https://doi.org/10.1073/pnas.2103605118
27. Zurek WH. Cosmological experiments in superfluid helium? Nature. 1985; 317(6037):505–508. https://doi.org/10.1038/317505a0